Deformation-free form error measurement of thin, plane-parallel optics floated on a heavy liquid

Jiyoung Chu,[1,2] Ulf Griesmann,[1,*] Quandou Wang,[1] Johannes A. Soons,[1]
and Eric C. Benck[3]

[1]National Institute of Standards and Technology, Manufacturing Engineering Laboratory,
Gaithersburg, Maryland 20899-8223, USA

[2]Samsung Electronics Co., 416 Maetan 3-dong, Yeongtong-gu, Suwon-si,
Gyeonggi-do, South Korea

[3]National Institute of Standards and Technology, Physics Laboratory,
Gaithersburg, Maryland 20899-8423, USA

*Corresponding author: ulf.griesmann@nist.gov

We describe a novel method for measuring the unconstrained flatness error of thin, plane-parallel precision optics. Test parts are floated on high-density aqueous metatungstate solutions while measuring the flatness error with an interferometer. The support of the flat optics by the uniform hydrostatic pressure at the submerged face of the flat optic eliminates flatness errors caused by mounting forces. A small, well characterized flatness error results from the bending of the floating flat by the hydrostatic pressure gradient at the edges. An equation describing the bending of thin, flat plates floating on a liquid is derived, which can be used to correct the flatness measurements of arbitrarily shaped plates. The method can be used to measure flatness errors of both nontransparent and transparent parts, and it is illustrated with flatness measurements of photomask blanks and substrates for extreme ultraviolet lithography. The refractive index of a saturated aqueous lithium metatungstate solution was measured at 632.8 nm and was found to be close to the refractive indices of several low thermal expansion optical materials.

OCIS codes: 120.3180, 220.4840, 220.3740.

1. Introduction

A central problem in precision form metrology is the separation of errors of the measurement instrument, for example, an interferometer, from the intrinsic form error of the surface under test. In addition, the form of optical precision surfaces is always affected by the forces from mechanical fixtures holding them. Forces due to mechanical clamping, chucking in vacuum or electrostatic chucks, and gravity cause surface deformations that must be either eliminated or calibrated. This is particularly important for thin, flexible parts when form error measurements with low uncertainty are desired.

Measurement algorithms, sometimes called "absolute tests," for the separation of instrument errors and mounting-induced errors from the form errors of the part under test have been developed for many years. Well known examples are the three-flat tests used for the calibration of interferometer reference flats (see, e.g., [1–3] and the references therein). However, error separation procedures cannot be found for all situations, and it is particularly difficult to characterize deformations of a surface due to mounting forces with an absolute test.

An example of thin flat optics that must be characterized with low uncertainty are photomask substrates and blanks for extreme ultraviolet (EUV) lithography (EUVL) at a wavelength of 13.5 nm. Photomasks contain the layout of an integrated circuit that is projected, usually demagnified 4:1, onto the wafer surface by an imaging system. EUVL photomask substrates are square with a standard width of 152 mm and a thickness of 6.35 mm as
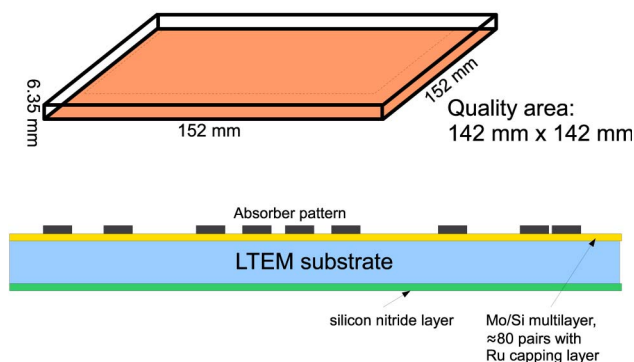
Fig. 1. (Color online) Dimensions of an EUVL photomask substrate and coatings on an EUVL photomask blank.

shown in Fig. 1. Several low thermal expansion materials (LTEM) with coefficients of thermal expansion $<0.03 \times 10^{-6}\,\mathrm{K}^{-1}$ are used to make EUVL photomask substrates. Within a quality area of 142 mm× 142 mm the peak-to-valley flatness error of front and back sides of an unconstrained EUVL photomask substrate must be as low as 30 nm for the highest quality substrates to achieve the very small pattern placement errors required in EUV lithography. These and other characteristics of EUVL mask substrates are described in a standard published by the Semiconductor Equipment and Materials International (SEMI) organization [4].

Coated but unpatterned photomask substrates are termed "photomask blanks." The flatness error of photomask blanks is strongly influenced by the coatings that are applied to the front and back surfaces because of coating stresses. The front surface of EUVL photomask blanks receives a reflective multilayer coating consisting of multiple Mo/Si layer pairs, a capping layer to reduce the diffusion of oxygen into the reflective multilayer, and possibly additional layers [4]. The back side coating facilitates the electrostatic chucking of the finished photomask.

One way of determining the intrinsic flatness errors of photomask blanks and substrates is to mount the parts in a kinematic mount and calculate the mounting-induced deformations using a numerical finite-element analysis (FEA). The calculated deformation can then be subtracted from the measured flatness error to yield the unconstrained flatness error. This approach was taken by Battula et al. [5], who have modeled the deformation of EUVL substrates with FEA and then sought to verify the models using different substrate mounts. It appears that the chief problem of the modeling approach lies in the difficulty of verifying the numerical model as long as the unconstrained flatness error of the mask substrate cannot be *measured*.

Evans et al. [6] have described a quasi-absolute optical test for separating the deformations of a transparent photomask substrate due to the mounting device, or chuck, from its intrinsic flatness error using a reversal method that can be implemented with Fourier transform phase-shifting interferometry. Using this method it was possible to separate the mounting-induced deformations from the intrinsic deformations of a mask substrate with the exception of the component in the combined flatness error with fourfold symmetry that is odd under reflections at the y axis. For high-quality photomask substrates this component is likely to be negligibly small. The main limitation of this test is that it can only be applied to transparent parts. The intrinsic flatness error of a coated photomask blank cannot be separated from mounting-induced deformations using the test by Evans et al. [6].

In this paper we describe a new method of separating the intrinsic flatness errors of flat precision parts from mounting-induced deformations that is suitable for measuring the flatness of both photomask blanks and substrates. By floating the mask substrate or blank on a heavy, high density liquid, mounting-induced deformations are essentially eliminated, and the unconstrained flatness error of the part can be measured directly. The unconstrained form error can then be used to determine the deformation of the part in a mount or chuck. We illustrate the method with flatness measurements of EUVL photomask blanks and substrates, but it is applicable to any precision flat for which a measurement of the unconstrained form error is desired. In Section 2 the properties of the heavy liquids that were used to float the test parts are summarized. In Section 3 the measurement setup is described, and several effects are analyzed that can bias the measurement. Sections 4 and 5 describe results of flatness error measurements of EUVL mask blanks and substrates.

2. Properties of Metatungstate Solutions

Metatungstates are a group of tungstates (tungsten compounds containing oxoanions) that have polyanions of the form $[H_2W_{12}O_{40}]^{6-}$ [7]. Lithium metatungstate (LMT, $Li_6[H_2W_{12}O_{40}] \cdot 3H_2O$) and sodium metatungstate (SMT, $Na_6[H_2W_{12}O_{40}] \cdot 3H_2O$) are highly soluble in water and other polar solvents. These metatungstate salts are only minimally toxic and can be used in a typical optical laboratory environment without special equipment for handling toxic materials. The saturated aqueous solutions contain about 15% water and have densities close to $3\,\mathrm{g/cm^3}$ at room temperature. This density is substantially higher than the density of many glasses and of low thermal expansion materials (see Table 2) that are used to make photomask substrates. Aqueous solutions of LMT and SMT are available commercially for applications requiring separation of materials with different densities, e.g., for the separation of fossils from minerals or to separate valuable minerals from sand and clay [8,9]. A similar heavy liquid, a lithium polytungstate (LST), containing a proprietary mixture of polytungstates dissolved in water, is also available commercially. Data on physical properties of the heavy liquids are scarce and had to be compiled from material safety data sheets and other technical information provided by the suppliers. Density and viscosity of the tungstate solutions at

room temperature depend on the concentration. We chose to use nearly saturated tungstate solutions with densities of about $2.9\,\text{g/cm}^3$. This density is about 30% higher than the density of the photomask materials and ensures sufficient buoyancy to prevent the top surface of a photomask from being submerged inadvertently in the fluid during handling. The properties of the commercially available aqueous tungstate solutions that are most important for our application are summarized in Table 1.

The refractive index of a saturated aqueous lithium metatungstate solution (LMT) at $2.95\,\text{g/cm}^3$ was measured at 632.8 nm, the wavelength of many phase-shifting interferometers used for form measurements, using the minimum deviation method as described by Burnett and Kaplan [10]. A hollow prism with plane parallel windows was filled with the LMT solution, and the deviation angles of light passing through the prism at minimum deviation were measured with a goniometer. Deviation angles were measured for light from a helium–neon laser at 632.834 nm and for the red spectral line emitted by a cadmium–argon low pressure discharge lamp at 643.847 nm. The measurements were made at the laboratory room temperature of 16.6 °C. The refractive index of the saturated LMT solution at 632.8 nm and its standard uncertainty, calculated from the standard deviations of the angle measurements, is 1.5888 ± 0.0002. Since the index n was measured at two closely spaced wavelengths λ, an estimate for the dispersion near 632.8 nm could also be obtained: $\mathrm{d}n/\mathrm{d}\lambda = (-7.5 \pm 2.6) \times 10^{-5}\,\text{nm}^{-1}$. The linear temperature dependence of the refractive index, $\mathrm{d}n/\mathrm{d}T$, was not determined, because it was not possible to control the laboratory room temperature sufficiently well.

The refractive index of the saturated LMT solution at 632.8 nm is much higher than the index of water (1.332, see [11]) and even slightly higher than the refractive indices of several low thermal expansion optical materials. For comparison, Table 2 lists the refractive indices of several low thermal expansion optical materials that were calculated from technical data provided by the glass manufacturers using a two-term Cauchy formula interpolation. As long as the density of the LMT liquid remains higher than that of a floating part, their refractive indices can be matched by diluting the liquid with water.

Stable metatungstate solutions are acidic [7] (see Table 1), which can be a problem if the surface of a part in contact with the solution is susceptible to corrosion. EUVL photomask blanks are unlikely to be

Table 2. Densities and Refractive Indices of Several Low Thermal Expansion Materials at 632.8 nm

Name	Density [g/cm³]	Refractive Index
Fused silica (generic)	2.201	1.45701 (see [21])
Corning ULE 7972[a]	2.21	1.4840
Schott ZERODUR[a]	2.55	1.5404
Ohara CLEARCERAM-Z[a]	2.53	1.5477

[a]Disclaimer: The full description of the procedures used in this paper requires the identification of certain commercial products and their suppliers. The inclusion of such information should in no way be construed as indicating that such products or suppliers are endorsed by NIST or are recommended by NIST or that they are necessarily the best materials or suppliers for the purposes described.

affected by the metatungstate solutions, because the rear surface of a mask blank is coated with silicon nitride, a material known to be highly corrosion resistant [12,13].

While liquids with lower viscosity are more desirable for the primary application of heavy liquids, mineral separation, a higher viscosity proved to be an advantage for the flatness measurements of mask blanks and substrates because a fluid with higher viscosity dampens residual motions of the photomask blanks more effectively, as is described in more detail in the following section. For the measurements described in this paper, the blanks and substrates were floated on LMT solution at a density of $2.95\,\text{g/cm}^3$.

3. Measurement Procedures

The flatness measurements of EUVL photomask blanks and substrates were made with the "eXtremely accurate CALibration InterferometeR" (XCALIBIR) at the National Institute of Standards and Technology (NIST). XCALIBIR is a versatile phase-shifting interferometer operating at a wavelength of 632.8 nm. The interferometer has a horizontal optical axis, and test parts are usually mounted vertically (on their edge). For the flatness measurements of floating photomask blanks and substrates, the interferometer was reconfigured so that the reference flat of the interferometer could be mounted above the photomask in horizontal orientation. A schematic of the XCALIBIR setup for the photomask blank and substrate measurements is shown in Fig. 2. The photograph inset in Fig. 2 shows the support structure for the fold mirror and the reference flat. On the left side of the photograph the collimator lens assembly is visible, which creates a collimated

Table 1. Properties of Aqueous Tungstate Solutions at Room Temperature

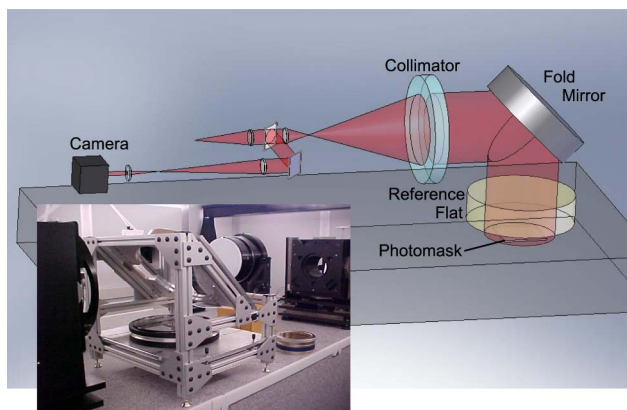| Name Abbreviation	Sodium Metatungstate (SMT)	Lithium Metatungstate (LMT)	Lithium Polytungstate (LST)
Formula	$Na_6[H_2W_{12}O_{40}] \cdot 3H_2O$	$Li_6[H_2W_{12}O_{40}] \cdot 3H_2O$	proprietary
Density ρ [g/cm³]		2.95	2.85
pH	≈3	≈4	≈4
Viscosity μ [mPa·s]	20 ± 1	36 ± 1	12 ± 1
n at 632.8 nm and 16.6 °C		1.5888 ± 0.0002	

Fig. 2. (Color online) Schematic of the XCALIBIR setup for photomask blank and substrate measurements. The inset photograph shows the actual setup of fold mirror and reference flat.

test beam of just over 300 mm diameter. The aluminized fold mirror has a diameter of 350 mm and sends the test beam downward to the reference flat, which is visible below the fold mirror in Fig. 2. The downward beam is vignetted by the fold mirror, resulting in the noncircular field of view shown in Fig. 3. The coating of the photomask blanks is highly reflective in the visible, and poor fringe contrast would result if the blank was measured against an uncoated reference flat. A reference flat coated with absorptive antireflection coating similar to a Clapham–Dew coating [14] was used for the measurements of both coated photomask blanks and uncoated substrates. This resulted in excellent fringe contrast for the highly reflective photomask blanks and acceptable fringe contrast for the uncoated substrates. XCALIBIR is equipped with a tunable single frequency diode laser, and phase measurements

were made by shifting the wavelength of the diode laser. For an interferometer resonator of length t the free spectral range $\Delta\lambda$ is

$$\Delta\lambda = \frac{\lambda^2}{2nt},\qquad(1)$$

where n is the refractive index of the medium filling the resonator and λ is the interferometer wavelength. A change in wavelength corresponding to the free spectral range is equivalent to a phase shift of 2π. During wavelength shifting the laser power is monitored and held constant to prevent measurement errors due to intensity variation.

A tray machined from a black acetal plastic filled with LMT was used to float the EUVL photomask blanks and substrates. The bottom of the tray was sandblasted to prevent specular reflections from the tray bottom in the measurements of transparent photomask substrates. Figure 4 shows an EUVL photomask blank floating on a tungstate solution. The internal width of the tray is 175 mm, and the corners are rounded with a radius of 10 mm. The standard width of photomasks is 152 mm. The gap of 11.5 mm on all sides of the photomask was considered sufficiently large to minimize effects due to the surface tension of the liquids on the flatness error of the parts under test. In preparation for a flatness measurement, between 90 mL and 100 mL of fresh tungstate fluid was slowly poured into the tray to avoid formation of air bubbles and the trapping of bubbles at the bottom of the tray. Bubbles that occasionally were found on the liquid surface after the tray was filled were suctioned off with a syringe. The photomask blank or substrate was then lowered onto the liquid by hand. Initially, two plastic pins at each corner of the photomask blank as shown in Fig. 4 were used to prevent lateral movement of the floating parts. Two pairs of pins were later removed to investigate effects of the pins on the flatness error of the blanks. For the measurements described in this paper two pairs of restraining pins at diagonally opposing corners were used. The space
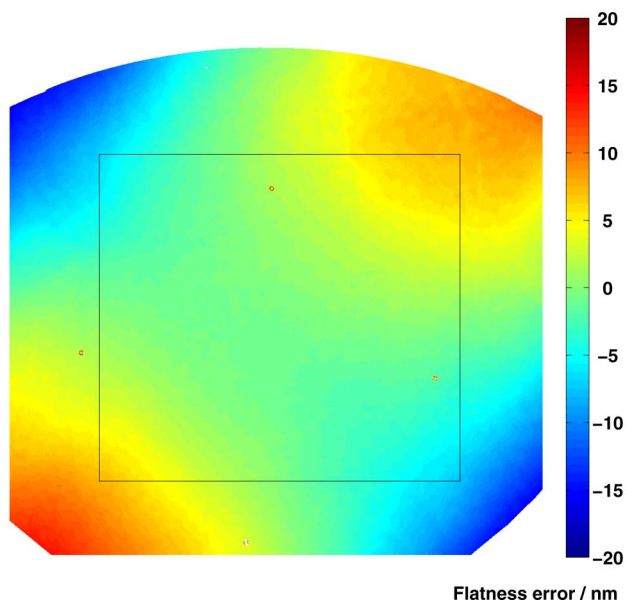

Fig. 3. (Color online) Flatness error of the reference flat shown in Fig. 2. The black square indicates the approximate size and location of the photomask blanks and substrates in the field of view of the interferometer.

Fig. 4. (Color online) EUVL photomask blank floating on a lithium metatungstate (LMT) solution.

between the pins and the photomask blank is a few tenths of a millimeter, and no force is exerted by the pins on the photomask blanks or substrates. Effects due to the surface tension of the heavy liquid were not observed. For example, flatness measurement results were identical when the tops of the restraining pins were above or below the fluid level. For a volume of 90 mL of LMT liquid in the tray, the distance between the photomask and the bottom of the tray is 1.8 mm and the photomask is immersed in the liquid to a height of 4.8 mm. Measurements were typically made shortly after lowering a part onto fresh LMT liquid to avoid problems resulting from water evaporation and crystal formation between the edge of a part and the restraining pins. Crystal growth was observed when a part was left in the liquid for an extended period of time, for example, overnight.

In the following subsections the residual deformation of a floating mask blank or substrate due to the hydrostatic pressure gradient in the fluid and the magnitude of thermal gradient effects is estimated. A calibration procedure for the horizontally mounted interferometer reference flat is also discussed, because it is an important contributor to the measurement uncertainty. Fluid dynamic effects in the heavy liquid were considered negligible. Test measurements with pure water in the tray, which is much less viscous than the heavy liquids, indicated no surface structures or disturbances that would suggest acoustic excitation of waves or currents in the liquid.

A. Hydrostatic Pressure Effects

While the hydrostatic pressure at the bottom of a floating photomask blank or substrate is nearly constant, a pressure gradient exists at the edges as shown in Fig. 5. The pressure gradient results in a uniformly distributed edge torque M that bends the flat. The deformation resulting from the pressure gradient at the plate edge can be calculated analytically for thin plates. For a flat plate of thickness t with density ρ_g floating on a liquid with density ρ_l, the liquid reaches a height z_l relative to the neutral plane of the flat:

$$z_l = t\left(\frac{\rho_g}{\rho_l} - \frac{1}{2}\right). \qquad (2)$$

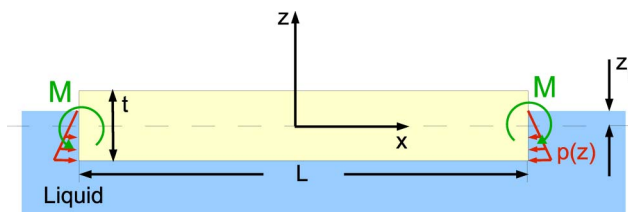The pressure distribution $p(z)$ exerted by the liquid on the edge of the flat is

Fig. 5. (Color online) Mechanical parameters of a thin plate floating on a liquid. The pressure gradient due to hydrostatic pressure at the edge of the plate is indicated in red.

$$p(z) = \begin{cases} 0 & \text{if } z \geq z_l, \\ \rho_l g(z_l - z) & \text{if } z < z_l, \end{cases} \qquad (3)$$

where g is the gravitational acceleration. The edge torque M per unit of edge length at the neutral plane ($z = 0$) of the plate equals

$$M = -\int_{-t/2}^{t/2} p(z)z\mathrm{d}z = -\int_{-t/2}^{z_l} \rho_l g(z_l - z)z\mathrm{d}z$$
$$= -gt^3\rho_g\left(\frac{\rho_g^2}{6\rho_l^2} - \frac{\rho_g}{4\rho_l}\right). \qquad (4)$$

The transversal deformation $w(x,y)$ of a *thin*, rectangular plate ($t \ll L$), subjected to a uniform edge torque M, and where the maximum deformation w_m is small compared to the thickness of the plate ($w_m \ll t$), is described by the equation [15]

$$w(x,y) = -\frac{M}{2D(1+\nu)}(x^2 + y^2), \qquad (5)$$

where D is the flexural rigidity,

$$D = \frac{Et^3}{12(1-\nu^2)}, \qquad (6)$$

E the elastic modulus of the plate material, and ν its Poisson ratio. Combining Eqs. (4)–(6) leads to an equation describing the deformation of a thin plate floating on a liquid by the hydrostatic pressure gradient at the edge:

$$w(x,y) = \frac{6(1-\nu)g\rho_g}{E}\left(\frac{\rho_g^2}{6\rho_l^2} - \frac{\rho_g}{4\rho_l}\right)(x^2 + y^2). \qquad (7)$$

It is worth noting that the deformation in Eq. (7) is independent of the plate thickness. The maximum (peak-to-valley) deformation w_m of a square flat with width L is given by

$$w_m = \frac{3(1-\nu)g\rho_g}{E}\left(\frac{\rho_g}{4\rho_l} - \frac{\rho_g^2}{6\rho_l^2}\right)L^2. \qquad (8)$$

For a square plate of width $L = 152\,\text{mm}$ made from a low thermal expansion material with elastic modulus $E = 67.6\,\text{GPa}$, density $\rho_g = 2.21\,\text{g/cm}^3$, and Poisson's ratio $\nu = 0.17$, floating on a liquid with a density of $\rho_l = 2.95\,\text{g/cm}^3$, the maximum deformation due to the hydrostatic pressure gradient at the edges is 1.7 nm. This result was corroborated by a finite-element model of the floating photomask blank. Calculating the uncertainty of the maximum deformation is complicated by the lack of uncertainty data for the material parameters, but an estimate of the typical uncertainty can be obtained based on plausible assumptions for the uncertainties of the variables in Eq. (8). When it is assumed that the density of the plate ρ_g, the elastic modulus E, and the width L of the plate are known with relative uncer-

tainties of 1%, and Poisson's ratio ν of the plate material and the density of the liquid ρ_l are known with relative uncertainties of 5%, and assuming Gaussian uncertainty propagation, the uncertainty for the maximum deformation is 0.05 nm. For many applications a small deformation $w_m = (1.7 \pm 0.05)$ nm can simply be neglected or it can be considered a contributor to the measurement uncertainty. If necessary, the deformation due to the hydrostatic pressure gradient $w(x, y)$ can be subtracted from the measured flatness error.

The distribution of the torque around the edge of a floating plate caused by the hydrostatic pressure gradient is independent of the shape of the plate, and it can be shown that Eq. (5) is valid for any shape [15]. Many optical components have a circular shape, and the maximum (peak-to-valley) deformation of thin, circular plates with radius R by hydrostatic pressure gradients at the edge is described by an equation similar to Eq. (7):

$$w_m = \frac{6(1-\nu)g\rho_g}{E}\left(\frac{\rho_g}{4\rho_l} - \frac{\rho_g^2}{6\rho_l^2}\right)R^2. \tag{9}$$

In the derivation of Eq. (8) it was assumed that the submerged face of the floating plate is perfectly flat. This assumption is only approximately valid, because the flat has a flatness error and the hydrostatic pressure will vary across the bottom of the plate. A peak-to-valley flatness error δz results in a pressure differential $\delta p_z = \rho_l g \delta z$. The ratio $\delta p_z / p(-t/2)$ of the pressure differential to the pressure at the bottom of the plate is about 2×10^{-5} for a peak-to-valley flatness error of 100 nm. The deflection of the plate caused by the pressure differential due to the flatness error was considered negligible.

A further nonuniformity of the hydrostatic pressure is caused by the spherical nature of the gravitational force. Gravity is directed toward the center of the earth, which results in a slightly nonuniform distribution of the gravitational force component normal to the flat surface. When it is assumed that the plate is rigid, which yields the worst-case pressure differential, the pressure differential $\delta p_g = \rho_l \delta g(z_l + t/2)$ resulting from the variation in the gravity component normal to the plate surface is small. For a 152 mm wide photomask blank floating on LMT, the ratio $\delta p_g / p(-t/2)$ of the pressure differential to the pressure at the bottom of the plate is about 1.7×10^{-8}. This pressure differential is much smaller than the pressure differential due to the flatness error, and the effect is negligible.

B. Effects of Temperature Gradients

Next to the hydrostatic pressure a temperature gradient can result in a deformation of a floating photomask blank or substrate. A temperature difference between the liquid and the surrounding air will result in a thermal gradient dT/dz in vertical direction in the glass, which causes a deformation with constant curvature. The deformation is approximately stress free, and a simple one-dimensional model

can be used to estimate the radius of curvature R. When one considers the difference Δl in the thermal expansion of two parallel fibers of the material parallel to the faces with length l, coefficient of thermal expansion α, and separated by a distance w, the difference Δl of the fibers due to the temperature gradient is

$$\Delta l = l\alpha w \frac{dT}{dz}. \tag{10}$$

The length difference Δl of the fibers due to a constant radius of curvature R is also described by

$$\Delta l = w \frac{l}{R}. \tag{11}$$

Combining Eqs. (10) and (11) yields an expression for the curvature $1/R$ of the plate:

$$\frac{1}{R} = \alpha \frac{dT}{dz}. \tag{12}$$

The resulting flatness error (sag) for a square plate of width L is

$$s \simeq \frac{L^2}{2}\frac{1}{2R} = \frac{1}{4}L^2\alpha\frac{dT}{dz}. \tag{13}$$

Eq. (13) can be used to estimate the worst-case flatness error of the floating photomask blank or substrate due to temperature gradients. The room temperature in the XCALIBIR laboratory is controlled at 20 °C. The temperature fluctuates by ± 0.05 °C around the set temperature. The coefficient of thermal expansion for the photomask material is approximately 0.03×10^{-6} K^{-1}, and the width of the photomask is 152 mm. The photomask thickness is 6.35 mm, and a worst-case thermal gradient of 0.1 K/6.35 mm can be assumed. Using Eq. (13), this thermal gradient leads to a flatness error of 2.8 nm. In practice the thermal gradient is likely to be much smaller because the poor heat transfer from air to the low thermal expansion substrate material will delay and reduce the creation of a thermal gradient in the material when the air temperature changes.

Another potential cause of a temperature gradient in the photomask is evaporative cooling of the heavy liquid during a measurement. A simple experiment was conducted to estimate the magnitude of the evaporative cooling. A small plastic beaker with 50 mm diameter was filled with 20 mL of saturated LMT solution at 2.95 g/cm^3 density. A thermistor temperature sensor was used to measure the temperature of the liquid. It was found that the temperature of the liquid dropped at a rate of about 0.006 °C/ min. Any effect of the cooling would first be observed at the edges of a photomask blank or substrate floating in the tray shown in Fig. 4, because the liquid under the part is not exposed to air. No indication of significant changes in the form error near the edge of a floating blank or substrate was found in repeat measurements. Figure. 6 shows the repeatability, pixel by pixel, of ten measurements that were made

over a period of about 30 min. It does not show a uniform worsening of the repeatability near the edges of the photomask blank.

C. Interferometer Calibration

A critical part of the measurement is the calibration of the horizontal reference surface. The reference flat had previously only been calibrated in vertical orientation, and it cannot be assumed that the reference surface remains unchanged after remounting the flat horizontally. An additional complication is that well known three-flat calibration procedures (see, e.g., [3]) could not be applied in this case because mechanical fixtures for rotating the flats in horizontal orientation were not available, and a reliable method for calibrating the sag of a horizontally mounted flat is not known. The reference flat was calibrated using overlapping measurements of a small flat with very low flatness error. The small flat is visible in Fig. 2 to the right of the support structure for reference flat and fold mirror. This flat has a diameter of 150 mm and a known peak-to-valley flatness error of 3.3 nm. The parabolic component (power and astigmatism) in the flatness error has a magnitude of only about 1 nm peak-to-valley. This flat was calibrated with the normal vector of the reference surface in a horizontal plane. It was then assumed that changing the orientation of the reference flat such that the normal vector is vertical results in a negligible change in the flatness error, because the flat is very thick (approximately 50 mm). The small flat was measured at seven overlapping locations that cover the whole aperture of the interferometer. At each location the flat was measured five times and after each measurement the flat was rotated by about 72° to approximately average out the flatness error without rotation symmetry in the small flat. All measurements were then stitched together, and the flatness error map of the reference flat shown in Fig. 3 was obtained. The flatness error of the reference flat is subtracted from the flatness error maps shown in Sections 4 and 5.

4. Photomask Blanks

For the photomask blank flatness measurements, the tray holding the heavy liquid and the blank (shown in Fig. 4) was placed on the optical table below the reference flat. The distance between the blank and the reference flat was about 10 cm. For a typical EUVL photomask blank, fringes like those shown in Fig. 7 were then observed with the interferometer. The measurements are complicated by the residual motion of the floating blank, which in the case of our experiment was caused by slow movements of the optical table of XCALIBIR. While the blanks and substrates are prevented from moving sideways, the movement of the optical table introduces a gradually changing tilt of the floating blank relative to the reference flat. The fringes, like those shown in Fig. 7, will slowly drift and lead to sampling errors in the phase measuring which, in turn, results in characteristic errors in the flatness measurements at twice the spatial frequency of the fringes. Another potential error source is the high reflectivity of the photomask blank coating that can result in multiple reflections between test surface and reference flat, resulting in higher harmonics in the fringe signal. We found that, despite the special coating on the reference flat, the observed fringes were not perfectly sinusoidal.

Measurement errors resulting from the residual motion of the photomask blank and higher harmonics in the fringes were reduced by over two orders of mag-
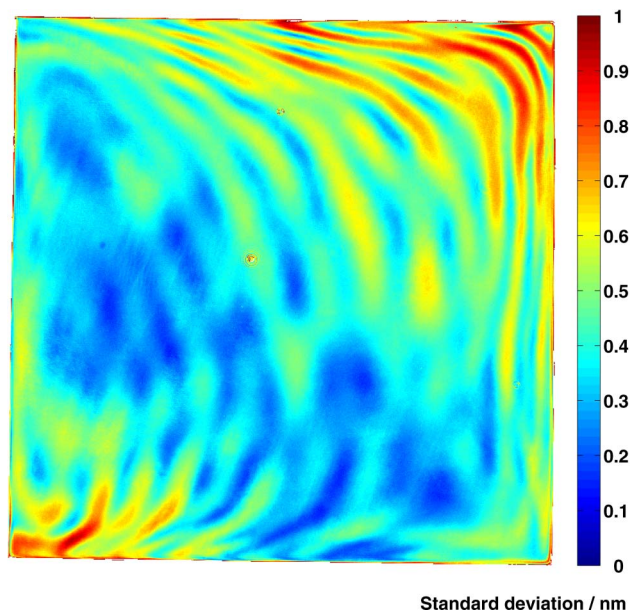

Standard deviation / nm

Fig. 6. (Color online) Repeatability map (standard deviation) of the blank flatness error calculated from 10 repeated measurements of the photomask blank flatness.
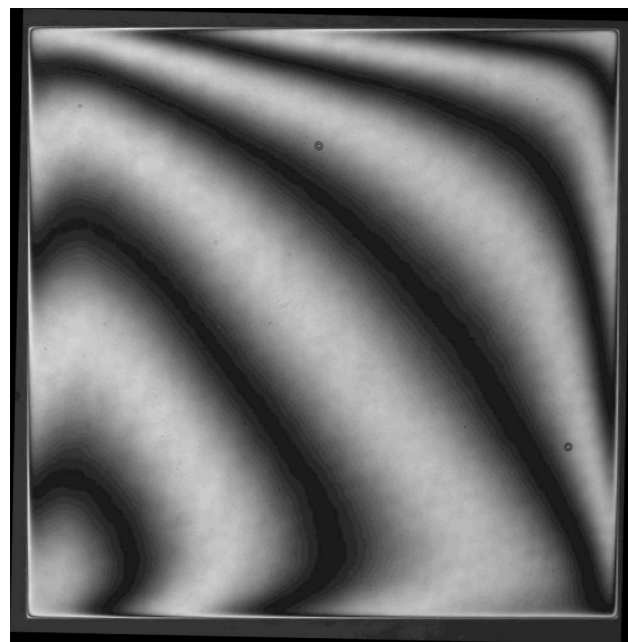

Fig. 7. Interferometer fringes of a photomask blank floating on a heavy liquid.

nitude by using a phase shifting algorithm that is insensitive to sampling errors and to higher harmonics in the fringe signal. The phase and amplitude response of the 13-sample phase shifting algorithm with 60° sampling increment that was designed for this measurement using the characteristic polynomial theory by Surrel [16] is shown in Fig. 8. This figure shows the first and second alias of the phase and amplitude response of the phase shifting algorithm. Like all algorithms with a sampling increment of 60°, this algorithm has a normalized Nyquist frequency of 3. The algorithm is not sensitive to the harmonic content of the fringe signal up to the 4th harmonic (blue line in Fig. 8). The phase response (red line in Fig. 8) is flat at the fundamental harmonic, which makes the algorithm insensitive to sampling errors due to the time-varying tilt of the floating mask blank. Table 3 lists the sampling coefficients for the 13-sample algorithm in the format introduced by Surrel [16]. Also listed is the loss factor η (see [17]) for the phase shifting algorithms used in the photomask blank and substrate flatness measurements.

Figure 9 is a false color map of the flatness error of the same EUVL photomask blank shown in Fig. 7. The form error of the reference flat is subtracted. The peak-to-valley flatness error within the quality area is approximately 100 nm. Ten measurements were made to evaluate the short-term repeatability of the measurements. Figure 6 shows a map of the pixel-by-pixel repeatability (one standard deviation) of the mask blank measurement in Fig. 9. This image reveals that the effects of the sampling errors due to the motion of the mask blank could not be completely eliminated, but the resulting spurious midfrequency ripple leads to an uncertainty of the flatness error measurement well below 1 nm for most of the photomask blank area. It must be emphasized that the ripple is not a feature of the measurement method but of the implementation.

Fig. 9. (Color online) Flatness error of the photomask blank (reference error removed).

The long-term repeatability was assessed by comparing two flatness error measurements of the same EUVL photomask blank made three weeks apart. The difference of the two measurements of the blank with the flatness error in Fig. 9 is shown in Fig. 10. The peak-to-valley of the difference is about 2.5 nm, and the root-mean-square (rms) of the difference map in Fig. 10 is 0.6 nm. The largest differences in repeat measurements were consistently found at the edges of the photomask blanks. This may be caused by the heat transfer into the mask blanks when they were loaded into the tray by hand. The circular features in the difference map Fig. 10 are residuals of the averaging procedure that was used for the cali-
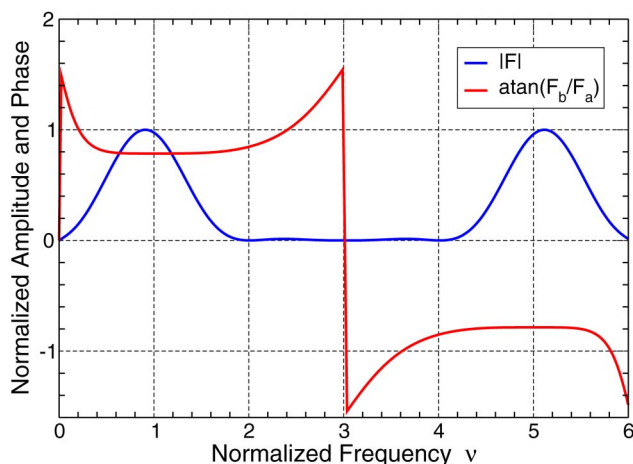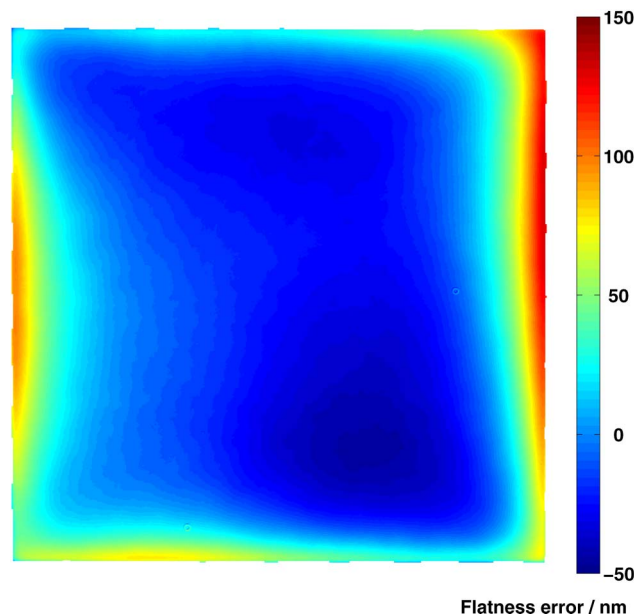

Fig. 8. (Color online) Phase response (red) and normalized sensitivity (blue) of the 13-sample phase shifting algorithm with 60° sampling steps used for the photomask blank measurements. $F_a(\nu)$ and $F_b(\nu)$ are the real and imaginary spectral transfer functions of the phase shifting algorithm.
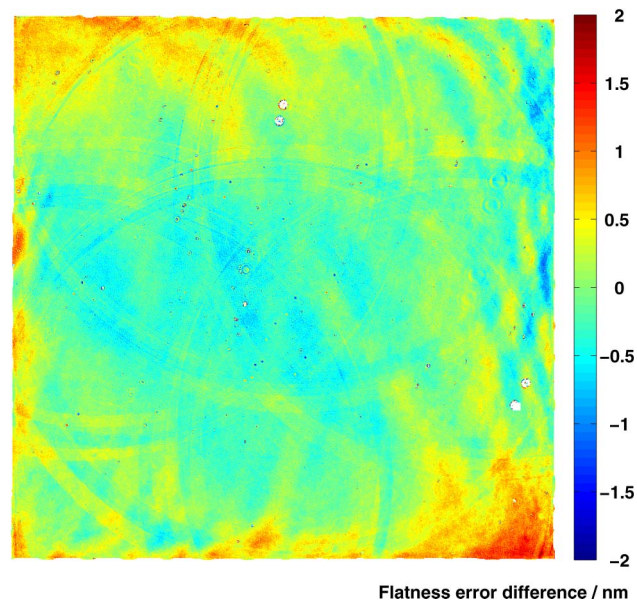

Fig. 10. (Color online) Difference of two measurements of the photomask blank of Fig. 7 made three weeks apart.

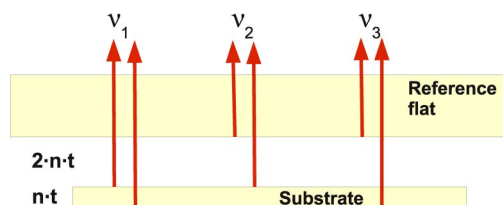Fig. 11. (Color online) Frequencies observed in wavelength shifting during photomask substrate measurements.

Samples	Sampling coefficients	η (see Ref. [17])
13	$\frac{[-1,-8,-11,10,43,46,0,-46,-43,-10,11,8,1]}{\sqrt{3}[1,0,-9,-18,-9,18,34,18,-9,-18,-9,0,1]}$	$\frac{108}{\sqrt{18239}} \simeq 0.8$
7	$\frac{[-1,-3,3,0,-3,3,1]}{\sqrt{3}[1,-1,-1,2,-1,-1,1]}$	$\frac{6\sqrt{3}}{\sqrt{119}} \simeq 0.95$

bration of the reference flat (see Subsection 3.C); they will not be present when an appropriate full-aperture calibration method is used.

5. Photomask Substrates

The method described in Section 4 for the flatness measurement of mask blanks can also be used to measure the flatness error of uncoated substrates. Substrate flatness measurements are a challenge because they are transparent and, as indicated in Fig. 11, several fringe systems are seen in the interferometer. In addition to the interference of light reflected by the reference surface and the front surface of the mask substrate, additional fringes are observed, which result from interference of reflections from the substrate's front and back surfaces and from interference of reflections from reference flat and substrate back surface. When the back surface of the photomask substrate is in contact with the heavy liquid, the fringe contrast of the unwanted fringes is much reduced, because the refractive index of the heavy liquid is close to the refractive index of the substrate material. If the refractive index of the photomask substrate is known, the heavy liquid can be diluted with water until its index matches the index of the substrate material, which eliminates the unwanted reflections. Since the material of the photomask substrate sample was unknown, the substrate was floated on the saturated LMT solution and wavelength shifting interferometry with a phase shifting algorithm that is insensitive to the fringes involving a reflection from the back surface of the substrate was used to filter out the unwanted fringes.

The basic concepts of measuring the flatness error of parallel plates with wavelength shifting interferometry are well known (see, e.g., de Groot [18] or Burke *et al.* [19]). For the flatness measurement the mask substrate was positioned so that the air gap between reference flat and front surface of the substrate was approximately twice the optical thickness nt of the mask substrate as shown in Fig. 11. Since the photomask substrate material was not known, a refractive index of 1.5 was assumed. When the wavelength is changed by one free spectral range for the cavity between the front and back surfaces of the substrate, it will be changed by exactly two or three free spectral ranges for the other two cavities. At the detector three frequencies are observed during wavelength shifting with exact frequency ratios: $\nu_1 : \nu_2 : \nu_3 = 1 : 2 : 3$. The signal containing the desired information about the substrate flatness is the 2nd harmonic ν_2. It can be measured with a phase shifting algorithm that is sensitive at the 2nd harmonic ν_2 and insensitive to the fundamental frequency ν_1 and its 3rd harmonic. The algorithm must also have a stationary phase response at the frequency ν_2. The phase and amplitude response of the seven-sample phase shifting algorithm with 60° sampling steps, which was designed for the measurement, is shown in Fig. 12. This algorithm is closely related to the Larkin–Oreb algorithm [20], and its sampling coefficients are listed in Table 3. The reason a much less robust phase shifting algorithm with only seven
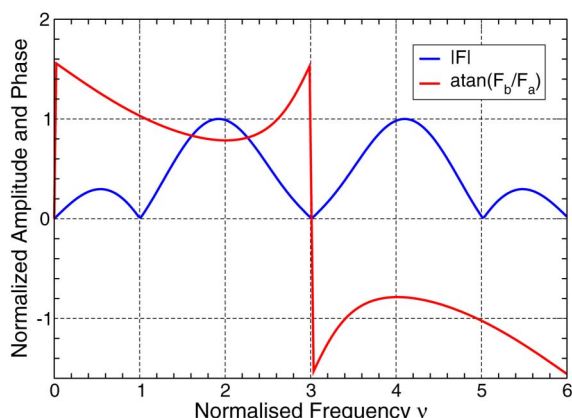

Fig. 12. (Color online) Phase response (red) and normalized sensitivity (blue) of the seven-sample phase shifting algorithm with 60° sampling steps used for the photomask substrate measurements.
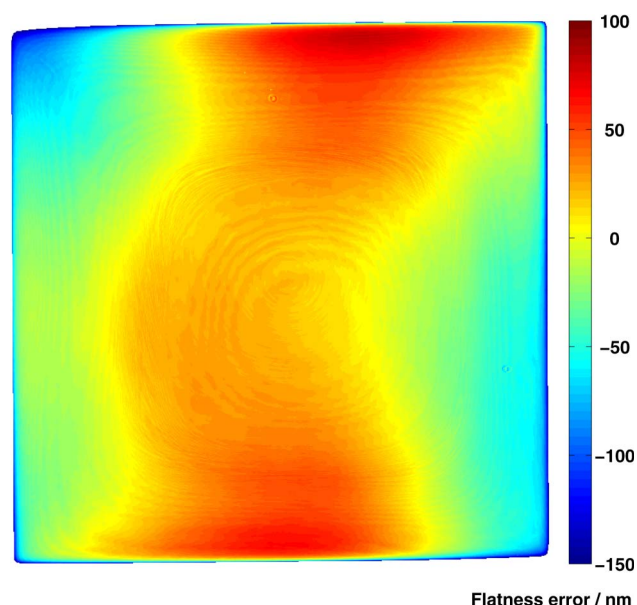

Flatness error / nm

Fig. 13. (Color online) Flatness error of the top surface of a photomask substrate floating on a lithium metatungstate solution (LMT).

samples was used for the mask substrate measurement is the limited tuning range of the laser. The free spectral range of the shortest interferometer cavity between the front and back surfaces of the mask substrate was almost as large as the maximum tuning range of the laser, which meant that phase shifts $>2\pi$ could not be realized and phase shifting algorithms with better phase response and better suppression of undesired frequencies, which require larger phase shifts, could not be used. The result of a flatness measurement of a floating EUVL mask substrate is shown in Fig. 13.

6. Conclusion

We have developed and demonstrated a new method for measuring the flatness error of thin, plane-parallel flat plates free from deformation by a mounting fixture that is applicable to both nontransparent and transparent parts. Instead of mounting the flats using a mechanical fixture, they are floated on a saturated aqueous lithium metatungstate solution during the measurement. This sidesteps the problem of having to separate the intrinsic flatness error of the plate from the flatness error introduced inadvertently by forces from the mounting fixture. In most cases the bending of the floating plate by the edge moment due to the hydrostatic pressure gradient at the edges will be negligible. A simple analytical model was derived to calculate the deformation due to the edge moment, which allows the measurements to be corrected for the hydrostatic pressure deformation. The new method is particularly valuable for flatness measurements of coated photomask blanks for EUV lithography because no other measurement procedures are known for separating the intrinsic flatness error of the blanks from mounting induced deformations. The high refractive index of the lithium metatungstate solution also simplifies the flatness measurement of transparent substrates. The liquid can be diluted to match the refractive index of the photomask substrate material to eliminate unwanted reflections from the back surface of the substrates as long as the density of the liquid remains higher than that of the test part. This obviates the need for wavelength shifting interferometry, and the flatness error of the front surface can be measured with conventional phase shifting interferometers.

References

1. J. Schwider, "Ein Interferenzverfahren zur Absolutprüfung von Planflächennormalen II," Opt. Acta **14**, 389–400 (1967).
2. M. F. Küchel, "A new approach to solve the three flat problem," Optik (Jena) **112**, 381–391 (2001).
3. U. Griesmann, Q. Wang, and J. A. Soons, "Three-flat tests including mounting-induced deformations," Opt. Eng. **46**, 093601 (2007).
4. "SEMI Standard specification for extreme ultraviolet lithography mask substrates," SEMI P37-1102 (Semiconductor Equipment and Materials International, 2002).
5. V. S. Battula, J. R. Zeuske, R. L. Engelstad, P. Vukkadala, A. R. Mikkelson, and C. K. V. Peski, "Mounting methodologies to measure EUV reticle nonflatness," Proc. SPIE **7470**, 747014 (2009).
6. C. J. Evans, B. Truax, and C. Smith, "Chuck induced deformations in euv mask substrate metrology," presented at ASPE Topical Meeting on Precision Mechanical Design and Mechatronics for Sub-50 nm Semiconductor Equipment, Berkeley, California, USA, 7–8 April 2008.
7. N. N. Greenwood and A. Earnshaw, *Chemistry of the Elements*, 2nd ed. (Butterworth-Heinemann, 1997).
8. S. T. Krukowski, "Sodium metatungstate; a new heavy-mineral separation medium for the extraction of conodonts from insoluble residues," J. Paleontol. **62**, 314–316 (1988).
9. W. P. C. Duyvesteyn, H. Liu, N. L. Labaso, and P. L. Shrestha, "Lithium metatungstate," U.S. patent 5,178,848 (1993).
10. J. H. Burnett and S. G. Kaplan, "Measurement of the refractive index and thermo-optic coefficient of water near 193 nm," J. Microlithogr. Microfabrication Microsyst. **3**, 68–72 (2004).
11. M. Daimon and A. Masumura, "Measurement of the refractive index of distilled water from the near-infrared region to the ultraviolet," Appl. Opt. **46**, 3811–3820 (2007).
12. P. D. Fuqua and J. D. Barrie, "Optical properties and corrosion resistance of durable silver coatings," Mater. Res. Soc. Proc. **555**, 85–90 (1998).
13. C.-T. Chu, P. D. Fuqua, and J. D. Barrie, "Corrosion characterization of durable silver coatings by electrochemical impedance spectroscopy and accelerated environmental testing," Appl. Opt. **45**, 1583–1593 (2006).
14. P. Clapham and G. Dew, "Surface-coated reference flats for testing fully aluminized surfaces by means of a Fizeau interferometer," J. Sci. Instrum. **44**, 899–902 (1967).
15. S. P. Timoshenko and S. Woinowsky-Krieger, *Theory of Plates and Shells*, 2nd ed. (McGraw-Hill, 1959).
16. Y. Surrel, "Fringe analysis," Topics Appl. Phys. **77**, 52–102 (2000).
17. Y. Surrel, "Additive noise effect in digital phase detection," Appl. Opt. **36**, 271–276 (1997).
18. P. de Groot, "Measurement of transparent plates with wavelength-tuned phase-shifting interferometry," Appl. Opt. **39**, 2658–2663 (2000).
19. J. Burke, K. Hibino, R. Hanayama, and B. F. Oreb, "Simultaneous measurement of several near-parallel surfaces with wavelength-shifting interferometry and a tuneable phase-shifting method," Opt. Lasers Eng. **45**, 326–341 (2007).
20. K. G. Larkin and B. F. Oreb, "Design and assessment of symmetrical phase-shifting algorithms," J. Opt. Soc. Am. A **9**, 1740–1748 (1992).
21. I. H. Malitson, "Interspecimen comparison of the refractive index of fused silica," J. Opt. Soc. Am. **55**, 1205–1209 (1965).